Linköping Studies in Science and Technology
Dissertation No. 987

Controlling the Formation and Stability of Alumina Phases

Jon Martin Andersson

Linköpings universitet
INSTITUTE OF TECHNOLOGY

Plasma and Coatings Physics Division
Department of Physics, Chemistry, and Biology
Linköping University, SE-581 83 Linköping, Sweden

Linköping 2005

Cover

Linköping autumn reflected through an α-alumina film grown at 280 °C.

Photograph taken on October 29, 2005.

Film grown on October 26, 2001.

ISBN: 91-85457-71-X

ISSN: 0345-7524

Printed by UniTryck, Linköping, Sweden, 2005

ABSTRACT

In this work, physical phenomena related to the growth and phase formation of alumina, Al_2O_3, are investigated by experiments and computer calculations. Alumina finds applications in a wide variety of areas, due to many beneficial properties and several existing crystalline phases. For example, the α and κ phases are widely used as wear-resistant coatings due to their hardness and thermal stability, while, e.g., the metastable γ and θ phases find applications as catalysts or catalyst supports, since their surface energies are low and, hence, they have large surface areas available for catalytic reactions.

The metastable phases are involved in transition sequences, which all irreversibly end in the transformation to the stable α phase at about 1050 °C. As a consequence, the metastable aluminas, which can be grown at low temperatures, cannot be used in high temperature applications, since they are destroyed by the transformation into α. In contrast, α-alumina, which is the only thermodynamically stable phase, typically require high growth temperatures (~1000 °C), prohibiting the use of temperature sensitive substrates. Thus, *there is a need for increasing the thermal stability of metastable alumina and decreasing the growth temperature of the α phase.*

In the experimental part of this work, *hard and single-phased α-alumina thin films were grown by magnetron sputtering at temperatures down to 280 °C.* This dramatic decrease in growth temperature was achieved by two main factors. Firstly, the nucleation stage of growth was controlled by pre-depositing a chromia "template" layer, which is demonstrated to promote nucleation of α-alumina. Secondly, it is shown that energetic bombardment was needed to sustain growth of the α phase. Energy-resolved mass spectrometry measurements demonstrate that the likely source of energetic bombardment, in the present case, was oxygen ions/atoms originating from the target surface. Overall, these results demonstrate that *low-temperature α-alumina growth is possible by controlling both the nucleation step of growth as well as the energetic bombardment of the growing film.* In

addition, the mass spectrometry studies showed that a large fraction of the deposition flux consisted of AlO molecules, which were sputtered from the target. Since the film is formed by chemical bonding between the depositing species, this observation is important for the fundamental understanding of alumina thin film growth.

In the computational part of the work, *the effect of additives on the phase stability of α- and θ-alumina was investigated* by density functional theory calculations. A systematic study was performed of a large number of substitutional dopants in the alumina lattices. Most tested dopants tended to reverse the stability between α- and θ-alumina; so that, e.g., Mo-doping made the θ phase energetically favored. Thus, *it is possible to stabilize the metastable phases by additives*. An important reason for this is the physical size of the dopant ions with respect to the space available within the alumina lattices. For example, large ions induced θ stabilization, while ions only slightly larger than Al, e.g., Co and Cu, gave a slight increase in the relative stability of the α phase. We also studied the stability of some of these compounds with respect to pure alumina and other phases, containing the dopants, with the result that phase separations are energetically favored and will most likely occur at elevated temperatures.

PREFACE

-"Sir, I found this spoon!"

-"Good work!"

Romans in Life of Brian (approx.)

This thesis presents the scientific work done during my PhD studies in the Thin Film Physics and Plasma & Coatings Physics Divisions at Linköping University, from August 2001 until December 2005. The work has been aimed at achieving control over aluminum oxide thin film growth, in particular crystalline phase formation and stability. This goal was approached by a combination of experimental studies of the alumina thin film growth process and theoretical phase stability calculations on alumina-based oxides. The thesis consists of six papers preceded by an introductory part. The work was financed through the Swedish Research Council (VR).

I have enjoyed the balance between scientific freedom and responsibility during these years; the reader will have to decide whether I managed to stay on the road or not.

Linköping, November 2005

LIST OF PAPERS

Here the six papers, which are included in the thesis, are listed together with the author's contribution to each of them.

Thin film growth and characterization:

I. Microstructure of α-alumina thin films deposited at low temperatures on chromia template layers

J.M. Andersson, Zs. Czigány, P. Jin, and U. Helmersson, J. Vac. Sci. Technol. A 22, 117 (2004).

II. Phase control of Al_2O_3 thin films grown at low temperatures

J.M. Andersson, E. Wallin, U. Helmersson, U. Kreissig, and E.P. Münger, manuscript submitted.

Author's contribution

I did all depositions, XRD analyses, nanoindentation, TEM sample preparation, and wrote the papers. I took a major part in the planning and discussions of the investigations, together with E. Wallin, P. Jin, E.P. Münger, and U. Helmersson, and assisted in the TEM and ERDA analysis done by Zs. Czigány (TEM) and U. Kreissig (ERDA).

Plasma analysis:

III. Molecular content of the deposition flux during reactive Ar/O_2 RF magnetron sputtering of Al

J.M. Andersson, E. Wallin, E.P. Münger, and U. Helmersson, manuscript submitted.

IV. Energy distributions of positive and negative ions during reactive Ar/O_2 RF magnetron sputtering of Al

J.M. Andersson, E. Wallin, E.P. Münger, and U. Helmersson, manuscript in final preparation.

Author's contribution

I did all measurements and wrote the papers. I took a major part in the planning of the studies and discussion of the results, together with E. Wallin, E.P. Münger, and U. Helmersson.

Computational phase stability calculations:

V. Effects of additives in α- and θ-alumina: an ab initio study

E. Wallin, J.M. Andersson, V. Chirita, and U. Helmersson, J. Phys.: Condens. Matter 16, 8971 (2004).

VI. Ab initio calculations on the effects of additives on alumina phase stability

J.M. Andersson, E. Wallin, V. Chirita, E.P. Münger, and U. Helmersson, Phys. Rev. B 71, 014101 (2005).

Author's contribution

I wrote the manuscript and did all calculations for Paper VI and did parts of the calculations and writing for Paper V. I took a major part in the planning of the studies and discussion of the results, together with E. Wallin, V. Chirita, E.P. Münger, and U. Helmersson.

ACKNOWLEDGEMENTS

Thank you, everyone who helped, guided, and supported me during these years! I know I am very lucky to have had all of you around me.

Ulf, thanks for "pulling" me into PhD studies and for being brave enough to give me a lot of freedom in my work. I have learned a lot! ***Peter***, thanks for your interest and for many very good discussions on physics! ***Vio***, thanks for introducing me to computer calculations and for your great eye for writing a paper. Thanks ***Ping Jin***, for giving me the inspiration to start working on low-temperature growth of alumina. ***Lars*** and ***Jens***, thanks for maintaining the thin film group such an excellent place to work.

Erik, it really has meant a lot to have you working with the same project. Thanks for being a friend with the right sense of humor and also for being the perfect "ball plank"! ***Jones***, thanks for many coffee and lunch breaks and discussions about "life science". I look forward to meeting you at the pool table some time!

Thanks ***everyone*** else in the Plasma & Coatings and Thin Film Physics groups for being an excellent work family and for enjoyable coffee-lunch-coffee-coffee routines. I won't name you all, but thanks especially to ***Inger***, ***Kalle***, and ***Thomas*** for always being happy and helpful, and for giving some "stability" to the group! And ***Zsolt***, thanks for all help with electron microscopy! Thanks ***Denis*** for always being positive and making your surroundings happy, and the "alumina people" ***David*** and ***Hans*** for continuing the oxidation process of the group.

My ***friends*** from “outside the Physics building”, thanks for all your friendship and support and for everything we have done and will do together. You mean very much to me!

Finally, my ***Elisabet***, thanks for all your love and for believing much more in me than I do myself. I love you very much! ***Mamma***, ***Pappa***, ***Lisa***, ***Petter***, and ***Olle***, thanks for all support and caring. I couldn’t have had a better family! Thanks also to my “second” families, ***Jonssons*** and ***Anderssons***, for making me feel so at home and comfortable with you, even though I don’t drive a Volvo (yet)!

And thank you, ***God***…

CONTENTS

I. INTRODUCTION

The science of alumina (Al_2O_3) is old and a tremendous amount of research work has been done over the years. For example, a database* search with the keywords “alumina” or “Al_2O_3” results in 58 000 hits from 1969-2005, i.e., more than 4 published works per day for the last 36 years. However, alumina was known long before that. Even in antiquity several naturally occurring forms of alumina were known, such as the mineral corundum and the gemstones emery, ruby, and sapphire.[1] Due to this long history of research most intrinsic properties of alumina are known, but even today a significant part of the published work deals with alumina materials science on a fundamental level. The main reason is arguably the complexity (and usefulness) of the alumina *polymorphs* (i.e., crystalline phases).

The most important, and common, polymorphs are denoted α, γ, θ, and κ. In addition to these, there are reports on more than twenty other crystalline phases.[1] The α phase is the thermodynamically stable polymorph and occurs naturally as corundum or sapphire, while the other phases are metastable in bulk form (but can still be produced in certain processes where thermal equilibrium is not reached, e.g., thin film growth). The differences in properties between the phases make them important in different applications. For example, the α and κ phases are widely used as wear resistant coatings due to their high hardness and thermal stability, while γ- and θ-alumina are more suited for catalytic applications due to

* INSPEC

their lower surface energies, leading to larger active surface areas available for catalytic reactions.

Even though α-alumina is thermodynamically stable at all temperatures up to its melting point, the metastable phases are frequently formed in growth experiments at temperatures below 1000 °C. The reason seems to be that the metastable phases are surface energy stabilized at the initial stage of growth.[2] If heated, diffusion mechanisms activate the irreversible transformation into the α phase. Thus, growth of α-alumina is traditionally made complicated by the need of very high temperatures, whereas the use of the metastable aluminas is limited to low temperatures. *The aim of the work done in this thesis is to investigate these issues in order to understand and control phase formation and stability during growth of alumina thin films.* More concretely, *achieving low-temperature growth of α-alumina and/or high-temperature stability of metastable aluminas are goals, which would be of great importance and would increase the range of possible applications of alumina.*

The alumina growth studies presented in the thesis are concerned with thin film deposition by magnetron sputtering. In sputter deposition, a flux of atoms and molecules are incident onto a substrate, where they chemically react and form a film. The formation of the film is thus influenced by deposition conditions such as the substrate temperature, the concentrations and energies of the depositing species, and the nature of the substrate on which the film is growing. Since we would like to control the properties of the grown film, the effects of changing these deposition conditions need to be understood.

The experimental part of the studies (Papers I-IV) is focused on low-temperature growth (below about 500 °C) of alumina thin films, aimed at attaining the α phase. The effect of the substrate and substrate temperature was investigated in Paper I, showing that α-alumina can be grown at very low temperatures (280 °C) by using a “template” substrate which promotes α phase nucleation. In Papers II-IV, the effect of the deposition flux was investigated by growing films (Paper II) and relating their properties to energy-resolved mass spectrometry measurements (Papers III and IV), which give information on both the nature and the kinetic energies of the film-forming species. Overall, these studies demonstrate that it is possible to control the phase of the grown films and that low-temperature growth of α-alumina is possible. Explanations for why the α phase forms under certain conditions are also given.

Papers V and VI present computational studies performed by using density functional theory (DFT), which allow detailed studies on the atomic level of energetic relative stability between phases or structures. In this work DFT is used to investigate how the introduction of

dopants affects alumina phase stability. As an atom of the alumina lattice is substituted by another element, the energy of the lattice will change due to differences in, e.g., chemical bonding and/or size of the substituting atom compared to the original. It is shown that depending on the substitutional atom, it is possible to increase or decrease the relative stability of the α phase and even make it less stable than the θ phase. Consequently, the results predict that it should be possible to control the thermal stability of doped alumina thin films in order to, e.g., increase the thermal stability of metastable alumina phases. It is difficult, however, to predict the exact effect of doping in an experimental situation, since it was also shown that phase separations of the doped aluminas are energetically favored, and will most likely occur at elevated temperatures.

The following chapters are structured as follows. First the methods used and the physics behind them are briefly described in Chapter II (experimental methods) and Chapter III (computational). Chapter IV is dedicated to a discussion of alumina properties and a review of previous research related to the thesis. Finally, in Chapter V I summarize my contribution to the field and try to put it into the context of previous works.

II. EXPERIMENTAL TECHNIQUES

This chapter describes briefly the experimental techniques used in the work. Section A deals with thin film growth and Section B presents the methods used for film and plasma analysis.

A. Thin film deposition - sputtering

Thin films are often grown by vapor deposition, i.e., the film is formed by condensation (chemical reactions) of a vapor at the *substrate*. The nature of the vapor and the condensation mechanism constitute the main differences between the two basic categories of vapor growth techniques, *chemical vapor deposition* (CVD) and *physical vapor deposition* (PVD). In CVD, the vapor consists of volatile gases that are allowed to chemically react to form the film material at the substrate and (gas-phase) rest products which are transported away. In PVD, which is the method used in this thesis, atoms/molecules of the material to be deposited are transferred, in vapor form, from a source to the substrate, where they bond and form a thin film.

The source of atoms/molecules in PVD is typically a piece of the material to be deposited. In *evaporation* the source material is heated and the vapor created is allowed to

condense at the substrate. In the method which has been used in this work, *sputtering*,* the atoms/molecules of the solid source (the *target*) are instead ejected from the target material towards the substrate through momentum transfer, by bombarding the target with energetic ions. In the following sections, the sputtering deposition process is described in some more detail.

1. Basics

The detailed picture of sputtering processes is rather complex, but the basic principles are straightforward:[3] a target material is bombarded by energetic ions, resulting in sputtering (ejection) of atoms/molecules. These deposit onto the substrate and a film is formed. In thin film deposition the source of the energetic ions is usually a low-pressure *glow discharge* or *plasma* (see next section), which is initiated and sustained between the target (cathode) and the deposition chamber walls (anode), using a process gas (typically Ar at a pressure of ≤ 1 Pa). As a high negative potential is maintained at the target, positive ions are accelerated from the plasma into the target, causing sputtering.

The efficiency of the sputtering deposition process largely depends on two process parameters, both of which depend on the specific combination of process gas and target material. These are the *sputter yield* and the *secondary electron yield*, i.e., the numbers of sputtered atoms and secondary electrons, respectively, which are produced per bombarding gas ion. The sputter yield depends on, e.g., the efficiency of momentum transfer, the cross section for collision, the binding energy of the target atoms, and the kinetic energy of the incoming ions.[4] The secondary electron yield is strongly correlated to the work function of the target material, i.e., low work function results in high yield. At constant power a higher electron yield means a higher current drawn and, thus, lower discharge voltage and sputter yield. A higher yield also means a larger electronic fraction of the current and, hence, a lower ionic current and sputter rate. Consequently, a high secondary electron yield generally reduces the sputter efficiency. In the case of Al and Al_2O_3, the sputter yield is higher and the secondary electron yield lower for Al, making sputtering from the metal much more efficient compared to the oxide.[5]

---

* To "*sputter*" = to "*spit or squirt from the mouth with explosive sounds*" or to "*utter hastily or explosively in confusion or excitement*" or to "*dislodge (atoms) from the surface of a material by collision with high energy particles*". The word originates from the Dutch word "sputteren". (Merriam-Webster Online, http://www.m-w.com)

2. The plasma

A plasma is characterized as a partially ionized, but macroscopically neutral, gas containing neutrals, ions, and electrons, with high enough concentrations of charged particles for significant Coulomb interaction to occur.[6] Another characteristic is a positive potential of the plasma (the *plasma potential*) relative to any surface in contact with it. This potential difference is caused by the higher velocities of the electrons in the plasma compared to the ions, causing an initial negative charge build-up on the surface. The negative charge then tends to repel electrons and attract positive ions from the plasma until equilibrium is reached at a certain negative potential, relative to the plasma potential. The region between the plasma and an adjacent surface, over which the potential changes, is called the *sheath*.

A sputtering plasma is sustained by applying a high negative voltage to the target (a few hundred volts), which causes ions in the plasma to be accelerated over the sheath toward the target. The resulting collisions give rise to, e.g., sputtering of target atoms and emission of secondary electrons. The electrons are accelerated away from the target to ionize (by direct impact) more gas atoms, which bombard the target and produce more sputtered atoms and secondary electrons. When equilibrium is reached, a steady-state discharge is sustained and a film is being deposited on the substrate (and on the chamber walls).

3. Magnetron sputtering

Practically all sputtering processes today use *magnetrons*.[7] The basic principle is to place magnets behind the target to create a magnetic field between the outer and inner parts of the target, as schematically shown in Figure 1. The electrons involved in the sputtering process are then trapped in this field close to the target, where they dramatically increase the degree of ionization and thus the sputter rate. Compared to non-magnetron sputtering this can increase the deposition rate by an order of magnitude. It also enables the use of lower pressures, which gives a more directional and energetic deposition flux due to less gas phase scattering. One drawback is a

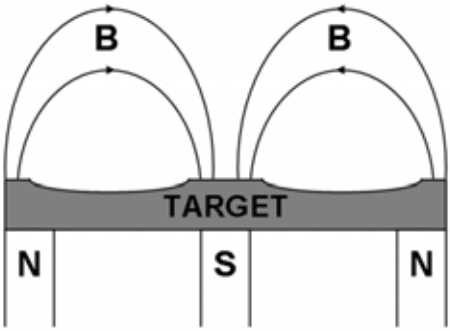

Figure 1. Schematic side-view cross-section of a sputtering magnetron, showing the magnetic field that traps the electrons close to the target and the erosion zone (“race track”) produced when sputtering.

non-uniform consumption of the target, since sputtering is concentrated to the area of highest electron density (the "*race track*"), i.e., where the magnetic field is parallel to the target surface.

4. Radio frequency sputtering

As mentioned previously, a compound alumina target was used in the work described in Paper I to grow films by sputtering. Since alumina is a very good insulator a direct current (DC) can not be drawn through it. Instead a *radio frequency* (RF) alternating current is used, which can be coupled through any target material, electrically conducting or not.[8] At these high frequencies (5-30 MHz), the relatively heavy ions are not able to follow the oscillations, while the lighter electrons are still moving easily with the current. A consequence is that they get enough energy from the RF field to ionize the sputtering gas, reducing the need for secondary electrons to sustain the plasma and enabling lower operating pressures compared to DC sputtering.

The reason why RF sputtering works is the *self-biasing* of the target to a negative potential of typically a few hundred volts. Due to this bias the resulting sputtering process is very similar to the case of DC sputtering. The self-bias is, in analogy with the plasma potential, explained by the much higher mobility of the electrons compared to the ions. During a positive half-cycle of the oscillating RF voltage, a large negative (electron) current will be drawn at the target, but during the following negative half-cycle only a small positive (ion) current flows, due to the low mobility of the ions. Therefore, initially a net negative current is drawn into the target. Since no charge can be transferred through the capacitively coupled target a negative potential (the target self-bias) builds up until no net current flows.

5. Reactive sputtering

When depositing compounds such as nitrides or oxides (e.g., Al_2O_3) by sputtering, it is not necessary to use a compound target. In *reactive sputtering*, which was used in the work of Papers II-IV, metallic targets (e.g., Al) are used and a reactive gas (e.g., O_2) is mixed into the sputtering plasma. This gas reacts with the metal deposited on the substrate to form the desired compound film.

The reactive sputtering process is made complex by reactions occurring not only at the substrate (forming the film), but also at the target and the chamber walls, as described by the well established Berg model.[9] These metal surfaces, which are kept "fresh" by the continuous sputtering/deposition, serve as an effective "extra pump", especially for systems of high reactivity such as Al sputtering in an $Ar+O_2$ gas mixture. The complexity of the

process is caused by this extra pump vanishing as the O_2 partial pressure is increased and the target surface becomes oxidized. This is illustrated in Figure 2; if the O_2 flow is increased to the point where the target shifts to oxidized mode (about 3 sccm in the figure), then the O_2 pressure increases strongly due to the decrease in pumping speed. When the flow is decreased again a lower flow (2 sccm) is needed before the target shifts back to the metallic state, causing the commonly observed *hysteresis* behaviour.[5] In order to enable operation of the process within the transition region between the metallic and oxidized modes, which is often desired, an active feedback partial pressure control system is generally needed.[10] However, under certain experimental conditions, e.g., if the pumping speed of the regular vacuum pump is very high or if the area of the sputtering target is small, then the importance of the extra pump is lessened.[9] In the deposition setup used in this work both these conditions were fulfilled and the hysteresis effects were not observed (Papers II-IV).

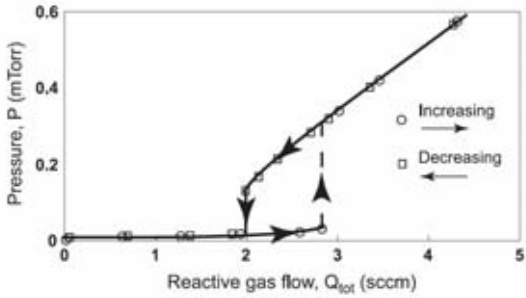

Figure 2. Illustration of the hysteresis behavior of the reactive gas partial pressure as a function of the gas flow. From Ref. 9.

6. Kinetic energies of sputtered particles

Through the collision cascade produced by the high energy ions (e.g., Ar^+) bombarding the target, the ejected particles gain a substantial kinetic energy. Thompson[11] derived an energy distribution for sputtered particles based on a simple model of random two-body elastic collision cascades within the target.[12] The Thompson distribution, shown in Figure 3, rises from zero at zero ejection energy to a peak at about half the surface binding energy and then falls off as ~$1/E^2$ at high energies. As stated by Thompson[11] this model is a simplification as it, e.g., assumes a planar surface potential and excludes such phenomena as focusing (due to crystal structure) and atomic binding, the latter presumably important at low energies.

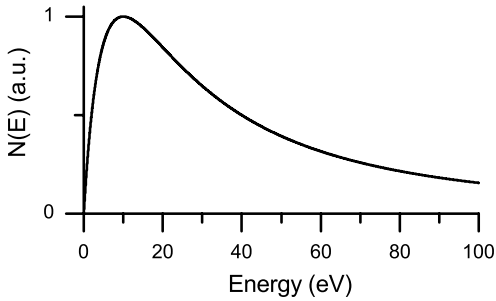

Figure 3. The Thompson energy distribution for sputtered particles plotted for a surface binding energy of 20 eV.

Nonetheless, a comparison with experimentally measured distributions shows that, in general, the agreement is fair; at least concerning the general shape of the distributions, see for example Refs. 13,14,15,16. Stuart *et al.*[14] measured the energy distributions of sputtered neutrals for a large number of target materials during sputtering by Kr^+ ions. They observed two trends: higher ejection energies for heavier target atoms and lower energies for higher sputter yields. Table 1 shows a summary of their measurements compared to the sublimation energies of the respective target materials.[*] Although there is a certain correlation between the most probable ejection energy and the sublimation energy, it is apparent that more factors than the surface binding energy are important when determining the position of the peak in the distribution.

Table 1. Experimental most probable ejection energies, E_{max},[14] during sputtering by 1.2 keV Kr^+, compared to target sublimation energies, E_{subl},[54] and sputter yields, S, for 0.5 keV Kr^+.[7] Stuart *et al.* have shown that E_{max} is the same for 0.6 keV as for 1.2 keV Kr^+.[14]

Target	Z	E_{max} (eV)	$E_{subl.}$ (eV/atom)	S (atoms/ion)
Be	4	0.3	3.32	0.48
Al	13	2.9	3.39	0.96
Si	14	2.3	4.63	0.50
Ti	22	4.2	4.85	0.48
V	23	2.3	5.31	-
Cr	24	3.5	4.10	-
Mn	25	1.8	2.92	-
Fe	26	3.7	4.28	1.07
Co	27	3.3	4.39	1.08
Ni	28	3.4	4.44	1.30
Cu	29	1.8	3.49	2.35
Ge	32	2.7	3.85	1.12
Zr	40	6.6	6.25	-
Mo	42	5.1	6.82	0.87
Rh	45	5.3	5.75	-
Pd	46	3.6	3.89	-
Ag	47	1.3	2.95	3.27
Ta	73	7.1	8.10	0.87
W	74	7.9	8.90	0.91
Re	75	10.3	8.03	-
Pt	78	4.8	5.84	1.82
Au	79	2.4	3.81	3.06
U	92	12.7	5.55	-

During sputtering of oxides or oxidized metals a certain amount of the sputtered particles can be negative oxygen ions.[17,18,19] Due to the high negative potential of the target

[*] The sublimation energies are often used as an estimate of the binding energies, due to lack of experimental data.

relative to the plasma, these are accelerated away from the target and will bombard the substrate during growth, if the pressure is low enough (and unless a very high negative substrate bias is used). This can strongly influence the growth behavior and, e.g., cause resputtering of the film.[17,20] In the work done for this thesis, it is shown that bombardment of energetic oxygen most likely promotes α phase formation during alumina thin film growth (Papers II and IV).

7. Nucleation and growth of thin films

A thin film is formed through chemical bonding between the atoms/molecules depositing onto the substrate/growth surface. The growth process (and, hence, the structure and properties of the grown film) is thus governed by deposition conditions such as the nature/temperature of the substrate and the contents/kinetic energies of the deposition flux.

a. The substrate structure strongly influences the nucleation stage of growth, since it defines the potential felt by the first layers of depositing species. For example, the use of single-crystal substrates can result in the growing film inheriting the structure of the substrate (*epitaxial growth*). In a similar manner a nucleation layer can be grown which functions as a "template" for the growing film, as in the work of this thesis where a chromia layer promoted α-alumina growth (Papers I and II). If the nucleation layer (or substrate) is polycrystalline, then the film can grow by *local epitaxy* onto the crystalline grains of the "template".

b. The content of the deposition flux is, of course, the main factor determining the composition of the film, but it can also influence the growth mechanisms. E.g., in deposition of compounds growth can proceed by either single atoms or molecular units, depending on the specific deposition conditions.[21,22] This can give rise to different bonding mechanisms and, consequently, structures of the grown films.[21] Paper III presents a study of the deposition flux contents during reactive sputtering of alumina, showing a large molecular fraction in the flux.

An advantage of sputtering over, e.g., evaporation, is that the sputtered flux of atoms will, at steady state conditions, have the same composition as the target, which is not as easily achieved for a melted source material. However, it is not necessarily true that the grown film has the same composition, since the probabilities of gas phase scattering or bonding to the growing film may be different for different species. Still, the composition of the target is often transferred to the film, making sputtering of compound targets widely used for, e.g., metal alloy deposition. It is also used in Paper I to grow alumina from a ceramic Al_2O_3 target.

c. The energy supplied to the growth surface determines, to a large extent, the microstructure and crystalline phase attained by the growing film. E.g., if the energy available to the depositing species is low, an amorphous and/or porous structure may result, since the low mobility of the atoms inhibit their movement to the optimal positions.

Energy can be supplied to the surface in several ways, most importantly by the substrate temperature and the kinetic energy of the plasma species. As discussed in Section II.A.6, sputtered atoms have a substantial kinetic energy when they are ejected towards the substrate (this is in contrast to evaporation where the evaporants have thermal energies). If the sputtering pressure is low enough, the energy from sputtering will be retained as the particles deposit onto the substrate. The resulting film structures as functions of temperature and pressure was first reported by Thornton[23] for sputtering of various metals, showing, e.g., that by increasing the energetic bombardment a certain film structure can be obtained at a lower temperature. His schematic zone diagram is shown in Figure 4. As is often the case, the growth temperature is given as the *homologous temperature*, i.e., relative to the melting temperature of the material. Although the dependence on growth parameters in a specific growth situation can be more complicated, the diagram gives a general idea on the dependence on pressure and temperature.

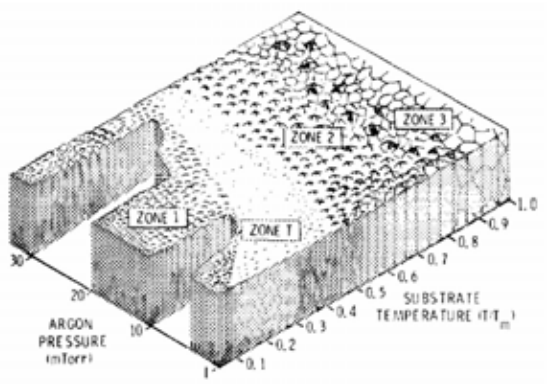

Figure 4. The Thornton zone diagram describing the microstructure of sputter deposited metal films as a function of pressure and substrate temperature. From Ref. 23.

The inherent energetic bombardment in sputtering can be further increased by utilizing the ions present in a plasma process. By applying a bias voltage to the substrate the positive ions close to the substrate are accelerated towards the surface of the growing film. In this way, energy (other than that from substrate heating) is supplied to the growth surface. This can, for example, enable growth at a lower substrate temperature than would otherwise be possible.[24] It has also been shown that such properties as microstructure,[25,26] defect density,[27] and crystal structure[28,29] can effectively be modified by energetic bombardment of the growth surface. Ion bombardment is especially utilized in the various *ionized PVD*

techniques, in which the ion to neutral ratio in the plasma is large (up to 100 % ions).[30,31] Then the energy of the depositing species themselves (i.e., not only the Ar ions) can be controlled by the applied bias. This can have important effects on crystalline phase formation of alumina thin films, as discussed in Section IV.B.2.

8. The deposition system

Any sputter deposition system is based on a vacuum chamber, due to the low operating pressures needed in the growth process. Usually a base pressure in the range of 10^{-4} Pa (*high vacuum*, HV) to 10^{-8} Pa (*ultrahigh vacuum*, UHV) is used. On one hand, a HV system is usually cheaper and more practical to work with. On the other hand, it is often desired to work at as low background pressure as possible, i.e., at UHV conditions, to avoid incorporation of residual gas impurities into the films. In certain applications, e.g., electronics, even very low levels of impurities might deteriorate the function of the film, so that low background pressures are essential. This is often true also in scientific research, since it is important to be able to separate the effect of a certain studied parameter from the effects of , e.g., the residual gas.

The deposition system (GG[*]) used in this work (Papers I-IV) is based on a UHV chamber evacuated by a 450 l/s turbomolecular drag pump. The ultimate pressure is about 10^{-8} Pa and the lowest base pressure used in this work was about 10^{-7} Pa. The system is equipped with three two-inch magnetrons, which can be placed in on-axis, 45° off-axis, and/or 90° off-axis positions with respect to the axis of sample rotation. The sample stage is rotating and movable so that the target-to-substrate distance can be varied in the range 5-25 cm (for an on-axis magnetron setup), and the substrate is heated by a resistive graphite heater to a maximum substrate temperature of about 900 °C. The temperature is measured during depositions by a thermocouple located behind the sample stage and was separately calibrated to a thermocouple attached to a clean silicon substrate surface. The process gases are introduced via mass flow controllers (O_2 and Ar) or via a leak valve (O_2 and, in Paper II, H_2O).

[*] GG = Ginnungagap. In nordic mythology Ginnungagap (="the wide open gap") was the empty space between Muspelheim and Nifelheim representing the original chaos (http://www.wikipedia.com).

B. Film and plasma analysis

In this section the analysis methods used in the thesis are briefly described.

1. X-ray diffraction

The method of *x-ray diffraction* (XRD) is probably the most used in the science of crystalline thin films. The simplest, and maybe most important, application of the technique is to determine the crystal structure of a sample. This can be done both for new materials, with the aid of simulations, and for previously known phases by comparison with reported data, as in Papers I and II.

In XRD, a beam of x-rays of a specific wavelength (often Cu Kα: 1.54 Å) is incident onto a sample and the resulting diffracted beams are detected. If the sample is crystalline, the detected intensity of diffracted beams will vary in different directions, depending on the interplanar lattice spacings, according to Bragg's law. By scanning incident (ω) and/or detecting (θ) angles (with respect to the sample surface) a unique diffraction pattern is produced, characteristic of the crystal structure of the sample. Since a relatively large volume of the sample is typically probed by XRD, it is a macroscopic method, in contrast to, e.g., *transmission electron microscopy* (TEM).

For polycrystalline samples, especially when the near-surface part of the material is of interest (e.g., the films studied in Papers I and II), it can be beneficial to use *grazing incidence* XRD. This means that the angle of incidence is kept fixed at a small (grazing) angle (about 2-5°) relative to the sample surface, while only the detecting angle is scanned. In this way a larger area and smaller depth of the sample is analyzed; i.e., a larger volume of the film material is probed.

2. Transmission electron microscopy

In TEM, an electron beam is focused, by electromagnetic lenses, onto the sample. The electrons which travel through the sample, i.e., the transmitted electrons, are detected and used to produce high-resolution physical images as well as diffractograms of the sample. As a consequence, both the microstructure and the crystalline phase of the sample can be determined by TEM, as was done in Paper I.

Since the penetration depth of the electrons is small, the sample has to be very thin; e.g., <100 Å for high resolution images.[32] This puts high demands on sample preparation, demands which are met by various procedures depending on the information desired and the type of sample studied. For the work of Paper I, the samples were prepared by first

mechanical grinding of the sample (down to a thickness of < 50 μm) and then by sputtering (ion milling) using an ion gun to produce thin regions for high resolution imaging.

The electron beam passing through the sample give rise to several detectable beams, one directly transmitted and others diffracted, producing a diffraction pattern of the sample. The undiffracted beam is used to produce *bright field* images of the sample showing the microstructure and, in high-resolution, the atomic structure. The diffracted beams give information on the crystal structure, similarly to XRD, but for a smaller and more localized area of the sample, hence the name *selected area electron diffraction* (SAED). It is also possible to produce so-called *dark field* images, in which one or more of the diffracted beams are selected to contribute to the image. It is then possible to determine, e.g., which grains in the film that have a certain selected crystallographic orientation.

3. Nanoindentation

For many applications, and especially for wear-resistant materials, it is of interest to measure mechanical properties. Such measurements involve many complex phenomena, sometimes making it difficult to distinguish between properties of the actual material and properties related to its microstructure or to the measurement equipment. Moreover, there are several methods to make and interpret the measurements and, hence, comparison between different measurements must be done with care.

The principle of *nanoindentation* is to press a diamond tip, with controlled force, into the sample surface and record the response of the material. The tip is allowed to penetrate, with increasing force up to a specified maximum load, and is then retracted, producing a load-unload curve like the one in Figure 5. From such curves properties like *elastic modulus* and *hardness* can be derived. Elastic modulus is an intrinsic property of a material, defined as the ratio stress/strain for a tensile stress acting in one direction. It can thus be different in different crystallographic directions depending on the isotropy of the material. Hardness is a measure of a samples resistance to penetration. It is not an intrinsic property as it is affected by, e.g., microstructure, and is thus more complex and more loosely

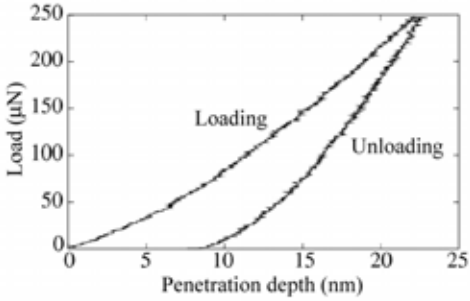

Figure 5. Typical nanoindentation load-unload curve for a polycrystalline α-alumina thin film.

defined than the elastic modulus. In this thesis (Paper I) the derivations of these values from the load-unload curves are done using the Oliver-Pharr method.[33]

When measuring thin films by nanoindentation, knowledge of the film thickness is important. If the tip penetrates too deeply, the measurements will be affected by the substrate. To avoid this, a rule of thumb is to keep the maximum penetration depth below about 10% of the film thickness.

4. Elastic recoil detection analysis

In thin film deposition the chemical composition of the grown films depend strongly on the growth conditions and, hence, it is important to be able to measure it accurately. In this work (Paper II) this was done by *elastic recoil detection analysis* (ERDA),[34] which can be described as a direct method of determining compositions.

The sample surface is bombarded by heavy energetic ions, in the present case 35 MeV Cl^{7+} incident at an angle of 15° with respect to the sample surface. These penetrate the surface region of the sample, causing recoils of the (lighter) atoms of the sample through elastic collisions. The recoils emerge from the sample in the forward direction and are detected; in the setup used here H was measured by a Si detector (with an Al foil stopping heavier atoms), while the Al and O recoils were detected in a Bragg ionization chamber. Since the elastic atomic collisions within the sample can be accurately modeled, the chemical composition of the film can be deduced from these measurements. In addition, since the energies of the recoils depend on the depth from which they originate, it is possible to achieve depth profiles, revealing any compositional changes appearing in the film. In this work the concentrations were found to be constant throughout the thickness of the film.

5. Energy-resolved mass spectrometry

The contents (Paper III) and energy distributions (Paper IV) of the ionic deposition flux were measured during sputtering by a differentially pumped *energy-resolved mass spectrometer*. The instrument is in contact with the plasma via a front plate, in the center of which a sampling orifice is placed (in the present measurements the diameter of the orifice was 300 μm). The front plate can be biased/grounded, but was kept at floating potential in this work due to the insulating oxide coating that formed on the probe during sputtering.

Within its separately pumped housing, the probe consists of five sections:

i. *Extraction.* Here, the ions from the plasma are extracted and guided into the probe by two electrodes, which are tuned to optimize the measurement for the specific plasma conditions used.

ii. *Ionization.* The next stage is the internal electron-impact ionization source, which can be used for analyzing, e.g., residual gases in the chamber. When studying the contents and energy distributions of the ionic deposition flux, however, this ionization source was turned off.

iii. *Energy filtering.* The ions are then guided into a Bessel box energy filter, a schematic of which is shown in Figure 6. Ions of a certain energy (A) will be guided through the filter by the voltages of the center stop/housing (V_1) and the end caps (V_2), while ions with lower (B) or higher (C) energies will be stopped.

iv. *Mass filtering.* After the energy filter the ions enter a quadrupole mass filter, which filters the ions according to their mass-to-charge ratio (m/q).

v. *Detection.* Finally, the ions are detected by a secondary electron multiplier.

The instrument can be used to produce a mass spectrum for ions of a specific energy or an energy distribution for ions of a certain mass (m/q). In this work (Papers III and IV), the probe was mounted at a typical substrate position so that the sampling orifice was facing the erosion track of the magnetron, in order to measure the ions which would be incident on a growing film.

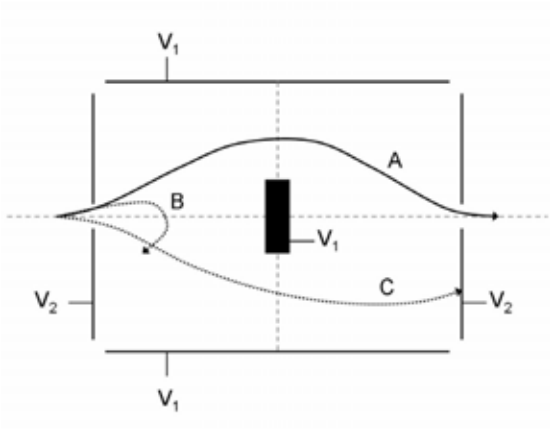

Figure 6. Schematic picture of the Bessel box energy filter. Ions of a specific energy (A) pass through, while ions of lower (B) or higher (C) energies are stopped.

The tuning of the electrode voltages (to optimize the measured signal) can be sensitive to the energies of the ions, so that the signal from ions of a certain energy are more amplified than those of other energies. In the measurements presented in this work, where a range of energies are of interest, the optimization was chosen to be less sensitive to a specific energy. This should yield a more realistic description of the physical situation, but it should still be stressed that energy-resolved mass spectrometry measurements are qualitative.

III. DENSITY FUNCTIONAL THEORY

Density functional theory (DFT) is probably the most commonly used method for calculating material properties from *first principles*, i.e., without any other input than the atomic numbers and positions. It is solidly based on quantum mechanics, making DFT calculations, in general, very accurate. This makes for a powerful computational method for predicting the behavior of materials, i.e., systems of atoms in various configurations and compositions. The main drawback of the method is the computational cost, which today limits the number of atoms studied to a few hundred on a supercomputer and about 50 on a work station.

This chapter gives a brief overview of the theory and the specific methods used in the thesis. For a more complete (and mathematical) treatment, the reader is referred to the original papers of Hohenberg, Kohn, and Sham,[35,36] and to the texts by Martin,[37] Sprik,[38] and Ruberto.[39]

A. The Hohenberg-Kohn theorems and the Kohn-Sham equations

The fundamentals of DFT are two theorems presented and proven by Hohenberg and Kohn[35] 40 years ago. The *first theorem* demonstrates that the external potential, $v_{ext}(\boldsymbol{r})$, in which the electrons move, is a unique functional of the ground state electron density, $n(\boldsymbol{r})$. Since the external potential fixes the Hamiltonian, H, this means that (in principal) all properties of the system are completely determined by the electron density (hence the name

density functional theory). Consequently, the total energy of the system can be expressed as a functional of the density, $E[n(\mathbf{r})]$. The *second theorem* states that the minimum of this energy functional is the ground state energy of the system and that the minimizing density is the exact ground state electron density. However, the problem remains that the functional is defined in terms of many-body wave functions, which depend on 3N variables for a system of N electrons. DFT, as described so far, is really "just" a reformulation of the difficult many-body problem.

The next step, which made DFT a success in practice, was made in 1965 by Kohn and Sham.[36] They made the *ansatz* that it is possible to replace the many-body system of interacting particles by an auxiliary system of independent electrons. This *ansatz* leads to the Schrödinger-like *Kohn-Sham equations*:

$$\left[-\frac{\hbar^2}{2m}\nabla^2 + e^2\int\frac{n(\mathbf{r}')}{|\mathbf{r}-\mathbf{r}'|}d\mathbf{r}' + v_{ext}(\mathbf{r}) + v_{xc}(\mathbf{r})\right]\psi_n(\mathbf{r}) = E_n\psi_n(\mathbf{r}).$$

The first term is the independent-electron kinetic energy, the second term is the Hartree potential, $v_{ext}(\mathbf{r})$ is the external potential in which the electrons move, i.e., the field from the atomic nuclei, and $v_{xc}(\mathbf{r})$ is the *exchange-correlation* potential, containing all the many-body contributions. For the case of a homogeneous electron gas the Kohn-Sham approach is exact and, based on the experience of workers who have used it over the years, the approach is valid also for more complex systems. Assuming that they are valid, the Kohn-Sham equations will give the exact electron density and ground state energy. Thus, instead of solving a many-body Schrödinger equation involving the total system wave function with 3N variables, the Kohn-Sham equations can be solved, involving only 3 variables! For these fundamental results, which have been very successfully applied in physics and chemistry, Walter Kohn was awarded the Nobel Prize in Chemistry 1998.

B. Exchange and correlation

The Kohn-Sham equations allow calculations of the exact ground state energy and electron density only if the exchange-correlation contribution is known, which, in general, it is not. Martin[37] suggests that the genius of the Kohn-Sham approach is that by separating out the single-electron kinetic energy and the long-range Hartree term, the remaining exchange-correlation contribution can be reasonably approximated as a local functional of the density.

1. The local density and generalized gradient approximations

The earliest approximation, which is still widely used, is called the *local density approximation* (LDA) and was introduced already in the original paper by Kohn and Sham.[36] In LDA the exchange-correlation energy is calculated in the same manner as if the system would have been a homogeneous electron gas, i.e., as a local functional of the density with the exchange-correlation potential at each point in space being the same as for a homogeneous electron gas of the same density. This is expected to be a good approximation for systems where the electron density is slowly varying, such as a nearly free electron metal, but significant errors should be introduced in inhomogeneous cases, e.g., free atoms. Hence, although the LDA works surprisingly well even in very inhomogeneous systems, there is a constant search for improvements.

Many attempts to improve the LDA have been based on the idea – also suggested by Kohn and Sham - to include, at each point, not only the electron density but also its gradient into the exchange-correlation energy functional. This idea should give more accurate results in inhomogeneous systems and has driven the development of the *generalized gradient approximations* (GGA), which in many situations give significantly improved results. There are several GGAs in use today and in this work (Papers V and VI) one of the most widely used forms, derived by Perdew and Wang[40,41] (called PW91), is applied.

C. Treating the electrons

By the application of the LDA or GGA, DFT is ready to be used in actual calculations. However, the calculations are still very computationally intensive and there is a need for physically reasonable simplifications. For example, the chemical bonds between atoms in a molecule/solid are almost exclusively formed by interactions between their valence electrons. In other words, an explicit treatment of the core electrons is not needed, as they remain practically unchanged whether the atom is free or part of a solid material (this is called the *frozen core approximation*). Since computational speed depends heavily on the number of electrons, this simplification dramatically reduces the cost.

1. Pseudopotentials and plane waves

The frozen core region is often treated through *pseudopotentials* (PPs), i.e., effective potentials which are calculated in an atomic calculation and then used to represent the core in calculations on molecules and solids. For efficient calculations it is necessary that the wave functions resulting from the PPs are as smooth as possible, since then a smaller number of

functions (e.g., plane waves) are needed to describe them. The traditional (norm-conserving) PP methods are quite accurate, but in a number of cases the resulting wave function is only moderately smoother than the full all-electron function, reducing their usefulness.[42] This disadvantage has to a great extent been removed by modern PP methods, such as the *ultra-soft pseudopotential*[43] (USPP) or the *projector augmented wave*[44] (PAW) methods, which are both used in this thesis. These approaches are based on the introduction of a smooth function, which is efficiently described by plane waves, and an auxiliary function localized around each ion, which represent the rapidly varying part of the density. Although the USPP and PAW methods are closely related, the PAW pseudopotentials are easier to construct and seem to give slightly higher accuracy, especially for magnetic materials.[42]

D. Computational details

This section discusses some considerations concerning the computational setup and the interpretation of results.

1. DFT setup used in this work

The DFT calculations within this thesis were performed with the Vienna *ab initio* simulation package (VASP).[45,46] This package uses plane waves to describe the wave functions and both USPP and PAW pseudopotentials are available, as well as LDA and GGA approximations of the exchange-correlation energy. In this work (Papers V and VI) the combinations PAW-GGA, USPP-LDA, and USPP-GGA were used, and comparisons were made between them.

2. The supercell

The atomic configuration of the system is defined relative to a *supercell*, which is repeated infinitely in space if *periodic boundary conditions* are applied (as in this work). For a calculation on perfect bulk it is usually sufficient to use the primitive unit cell of the lattice as the supercell. However, if a defect is introduced (e.g., an ad-atom on a surface or a dopant atom), it might be of interest to increase the size of the supercell in order to minimize unwanted interactions between the periodic replicas. A larger supercell can also be necessary, e.g., in calculations on dopants (Papers V and VI) in order to enable lower dopant concentrations (since at least one dopant atom has to be introduced into the cell). Often a reasonable compromise between accuracy and time consumption has to be accepted.

3. Stability calculations

Energy is a relative quantity. Therefore, the energy calculated for a certain system has to be compared to another system with the same atomic composition. For example, the *cohesive energy* of a metal is calculated as the difference between the energy of an atom in the bulk and the energy calculated for the free atom, while for oxides (e.g., Al_2O_3) it is common to calculate *formation energies* by comparing the energy of the oxide to the energies of bulk metal (e.g., fcc Al) and molecular oxygen, which are the most stable forms of the oxide constituents. Furthermore, in the case of dopant calculations (as in Papers V and VI) it is not possible to compare directly the energies of systems with different dopants or dopant levels, since then the systems do not contain the same atoms. Naturally, however, the relative stability between two crystalline phases of the same stoichiometry is calculated by directly comparing their respective energies.

4. Temperature in DFT calculations

All DFT calculations are made at 0 K.[*] When comparing with experiments this can be impractical since the temperatures of interest are often room temperature or higher. At these temperatures entropy contributions can be important and, thus, it is not always correct to assume that DFT results are still valid. Nonetheless, the calculated relative energetic stability between bulk structures is often used also at higher temperatures, with the motivation that the entropy contributions to the relative energy should be small. Given the success of DFT in confirming and predicting stability, this approach seems valid. For molecular systems, however, the entropy contributions are significantly larger and more important. This is the case, e.g., in Paper VI, where the stability of oxides in the presence of molecular oxygen is investigated. In such cases, the experimentally measured entropy of the molecular species can be included into the stability calculations.

5. Electronic structure

As described above, solving the Kohn-Sham equations yields the exact total energy and electron density of the system. Thus, the charge density can be visualized and used to draw qualitative conclusions on the bonding behavior between the atoms in the molecule/solid. An example calculated for θ-alumina is shown in Figure 7 where the ionic

[*] In DFT molecular dynamics simulations, however, temperature is included through the atomic motion according to the classical Newton's equation of motion, using forces calculated by DFT.

nature of the bonds is seen through the localization of charge around the oxygen nuclei, while almost no valence electrons are seen around the Al nucleus.

In many situations it is important to get information also on the *density of states* (DOS). This is, in principle, not possible by DFT, since the Kohn-Sham wave functions and eigenstates do not correspond to those of the real physical system. Nonetheless, numerous researchers (including the present author) do present DOS calculated by DFT. The reason is that such results are usually fair representations of the true situations, although there is no theory supporting it (to the knowledge of the author). The interpretation has to be done with care, though, since the results come from the "artificial" single-electron system. For example, a common deficiency of DFT-calculated DOS is a large underestimation of band gaps for semiconductors and insulators.

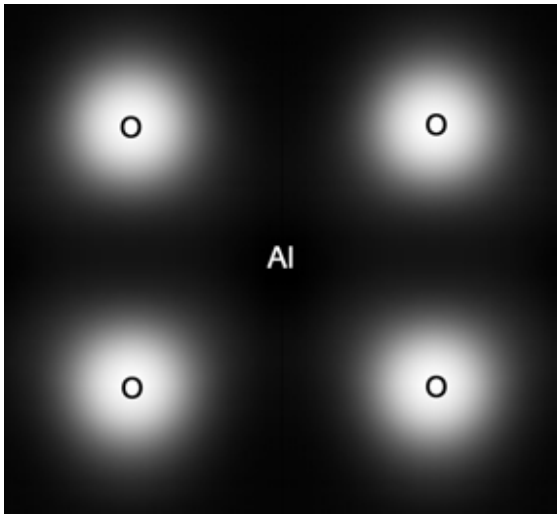

Figure 7. Charge density cross section in θ-alumina. The slice is made through the Al and O atoms in the mirror plane of an oxygen octahedron. Black corresponds to zero charge.

IV. ALUMINA

In this chapter the ceramic material *alumina*, or Al_2O_3, is introduced. The properties of alumina are described in the first section and then previous alumina research related to the thesis is presented.

A. Properties of alumina

Alumina has many appealing properties which makes the material interesting for applications in many different areas. For example, it is hard, stable, insulating, transparent, beautiful, etc. This section describes briefly the complexity of alumina crystalline phases and reviews the properties of the three phases which are encountered in this work.

1. Alumina polymorphs: a conundrum

Alumina exists in a number of crystalline phases (polymorphs), three of the most important being γ, θ, and α.

The α structure is thermodynamically stable at all temperatures up to its melting point at 2051 °C, but the metastable phases (e.g., γ and θ) still appear frequently in alumina growth studies for reasons that are discussed in the following sections.

The common alumina polymorphs can all be formed within typical synthesis temperatures, i.e., from room temperature up to about 1000 °C. This complicates the study and growth of alumina, since it becomes difficult to control the process so that the desired

phase is achieved. But the polymorphism also opens many opportunities for applications in various areas of technical science, since the properties of one alumina phase in some respects differ from the properties of another,[47] as described in the following sections. A summary of alumina properties is presented in Table 2.

Table 2. Selected properties of α- and θ-alumina (fu = chemical formula unit).

	α-Al_2O_3	θ-Al_2O_3	γ-Al_2O_3
Density (kg/m^3)	3980,[48] 3990[47]	3560,[48] 3600[47]	3200[48], 3700[47]
Elastic modulus (GPa)	409,[48] 441[33]	-	-
Hardness (GPa)	28[33]	-	-
Bulk modulus (GPa)	239[49]	-	-
Band gap (eV)	8.8[57]	7.4[60]	-
Melting point (°C)	2051[48]	θ → α: 1050 °C[47]	γ → δ: 700-800 °C[47]

Structural properties of α-Al_2O_3[53]

Space group	$R\bar{3}c$ (rhombohedral, two fu/cell)
Lattice parameters	a=5.128 Å, α=55.33°, V=42.6 Å^3/fu
Internal coordinates	Al: (4c) ±(u, u, u; u+½, u+½, u+½), u=0.352
	O: (6e) ±(w, ½-w, ¼; ½-w, ¼, w; ¼, w, ½-w), w=0.556

Structural properties of θ-Al_2O_3[50, 58]

Space group	$C2/m$ (monoclinic, four fu/cell)
Lattice parameters	a=11.85 Å, b=2.904 Å, c=5.622 Å, β=103.8°, V=47.0 Å^3/fu
Internal coordinates	All atoms: (4i) ±(u, 0, u; u+½, ½, w), with:

Atom	u	w
Al1	0.917	0.207
Al2	0.660	0.317
O1	0.161	0.098
O2	0.495	0.253
O3	0.827	0.427

Structural properties of γ-Al_2O_3[47]

Space group	$Fd\bar{3}m$ (defect cubic spinel structure, 32 fu/cell)
Lattice parameters	a≈7.9 Å, V≈46.2 Å^3/fu
	This structure is not well defined, but is usually characterized as an fcc O lattice with a partially random distribution of Al.

All alumina phases are involved in transformation sequences, which all have in common that they end in the α phase at high temperature. Figure 8 shows some phase transition relations for the common alumina phases. The transformations to the α phase are irreversible and typically take place at above 1000 °C.[47,51]

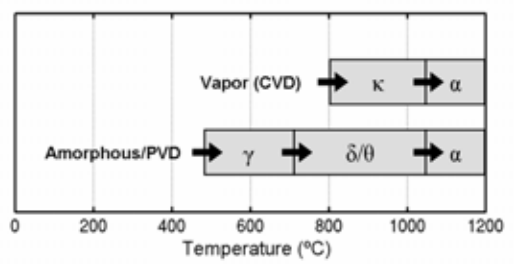

Figure 8. Selected transition sequences of alumina phases. For a more complete overview see, e.g., Ref. 39.

2. Properties of α-alumina

The α form of aluminum oxide is also known as *corundum* (the name comes from the naturally occurring mineral corundum, which consists of pure α-Al_2O_3). It is transparent and uncolored and is known in its single crystal form as *sapphire*. It is used not only in materials science, but occurs also as gemstones. The gem known as ruby is α-alumina doped with small amounts of chromium, while the gemstone sapphire is actually α-alumina doped with iron and titanium.

Like all alumina phases the α phase is highly ionic with calculated valences of +2.63*e* and –1.75*e* for aluminum and oxygen, respectively.[52] Thus the chemical bonds between ions are almost purely ionic (or electrostatic), similarly to the case of θ-alumina shown in Figure 7, a fact that is closely related to the structural behavior of alumina.

The corundum structure is also formed by a number of other metal sesquioxides, such as Cr_2O_3, Ti_2O_3, and Fe_2O_3.[53] The structure belongs to space group $R\bar{3}c$ and is rhombohedral with two formula units (10 atoms) in the primitive unit cell. However, a more often used unit cell is the hexagonal representation containing six formula units.[53] The *c* axis of the hexagonal cell is along the (111) direction of the rhombohedral lattice. The corundum structure can be described as a hexagonal close-packed (hcp) oxygen sublattice, in which the aluminum atoms, or ions, occupy two thirds of the octahedral interstices, i.e., they have six oxygen nearest neighbors. There is thus only one coordination (octahedral) for aluminum and one for oxygen (with four surrounding aluminum ions).

The thermodynamic stability of α-alumina makes it the most suited phase for use in many high-temperature applications, although also the κ phase is used due to its high transformation temperature. Other important characteristics of α-alumina are chemical inertness and high hardness. As seen in Table 1, the elastic modulus and hardness are measured to be ~440 and ~28 GPa,[33] respectively. These can be compared to diamond, which have values of ~1100 and ~100 GPa,[54] to TiN with values similar to those of α-alumina,[55] and to metallic Al, which has values of ~70 and ~0.3 GPa.[33,54] Combined, these properties has made α-alumina thin films important as, e.g., wear-resistant[24] and high-temperature diffusion barrier[56] coatings. Other uses of α-alumina is in electronics, where it is used, e.g., as an insulator due to the wide band gap of 8.8 eV,[57] and in optics, since it is completely transparent and stable at high temperature.

3. Properties of θ-alumina

The θ phase of alumina is metastable and transforms into the α phase at about 1050 °C.[47] It is less dense than the α phase with a density of about 3600 kg/m^3 compared to 4000 kg/m^3 for α-alumina.[47] Table 2 shows a collection of θ-alumina properties.

The structures of all alumina phases are built up around (slightly distorted) close-packed oxygen lattices and while the α phase has an hcp framework, the θ structure is based on an fcc oxygen lattice.[58] Within this oxygen framework, half the aluminum ions occupy octahedral interstitial sites and half occupy tetrahedral (with four oxygen neighbors) sites, as shown in Figure 9. This is also in contrast to the α phase. The oxygen ions have three different possible surroundings, each of which is occupied by one third of the oxygen ions. Two of these oxygen sites there have three aluminum nearest neighbors and the third has four. The structure is monoclinic, belonging to space group C2/m, and the unit cell contains four formula units (20 atoms) with lattice parameters as shown in Table 2. θ-alumina is a structural isomorph of β-Ga_2O_3 and, interestingly, gallium oxide can also form the corundum structure.

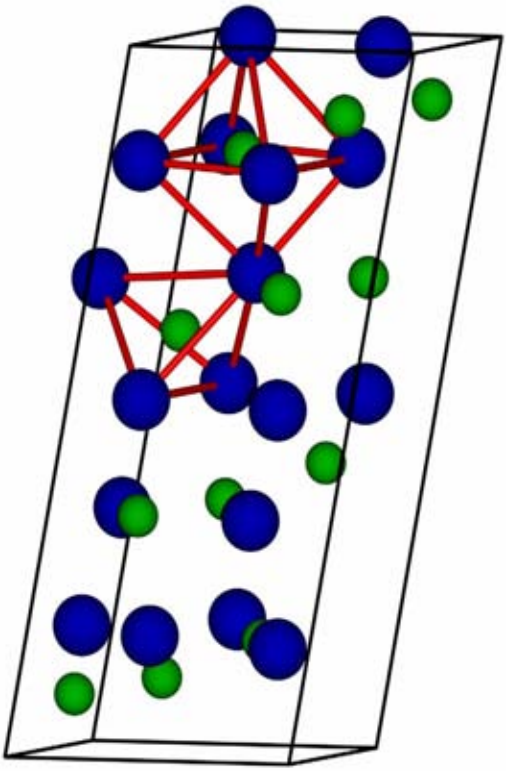

Figure 9. The θ-alumina monoclinic unit cell. Large spheres represent O atoms and small Al. Examples of tetra- and octahedral Al positions are indicated.

There are not as many investigations made on the θ phase as on α-alumina. It is clear, though, that it is highly ionic[59] and insulating with a band gap of 7.4 eV.[60] In DFT calculations, as in Papers V and VI, the θ phase is often chosen as a representative of the

metastable alumina phases. The reason is the well defined crystal structure, in contrast to, e.g., γ, and the structural similarities between the metastable phases.

4. Properties of γ-alumina

Due to low surface energy and, hence, high surface area, γ-alumina is extensively used as catalyst supports.[47,61] The low surface energy also means that the γ phase is surface energy stabilized when the surface area is high relative to the bulk volume, e.g., for small grain sizes.[2] The consequences on thin film growth are further discussed in Section IV.B.3. In high-temperature applications a problem with the use of the γ phase is that it transforms into θ at 700-800 °C.[47] This has led to the experimental research on doping of alumina to increase its thermal stability (see Section IV.B.5).

The γ-alumina structure has two main similarities with the θ phase, the fcc oxygen lattice and the mixture of octa- and tetrahedrally coordinated aluminum ions. However, the exact structure is not well defined. It is commonly believed that the structure can be described as a defect cubic spinel with the aluminum ions more or less randomly distributed between octa- and tetrahedral sites.[62] This makes DFT calculations on γ-alumina problematic and is the reason for choosing the θ phase as a representative of metastable aluminas (e.g., in Papers V and VI).

B. The alumina research field

This section contains a brief overview of related research previously done on alumina.

1. Alumina as a wear-resistant coating

Over the last decades, thin films have found an increasingly important application as wear-resistant coatings on, e.g., cutting tools. An important example is TiN,[63] which dramatically increased the life time of cutting tools. A drawback with TiN is the limited oxidation resistance at elevated temperatures. Later on this problem was dealt with by introducing Al into the TiN lattice[64] and thereby promoting the formation of a protective alumina layer through oxidation. Alumina thus find uses as a naturally formed protective layer on top of a hard material, but it is also synthesized, usually by CVD, and successfully used as a hard coating in itself.[65,66,67] Due to the competition between α and κ phase formation, it was traditionally difficult to synthesize high quality α-alumina films. However, recent developments have enabled precise control over the phase content of the coatings, giving significantly improved properties.[65] The growth of α-alumina, whether by CVD or

PVD, typically requires temperatures above 1000 °C,[66] which limits the choice of substrate material to those that can withstand high temperatures. These temperatures can also induce unwanted chemical effects.[68] Thus, a further physical understanding of alumina growth, aiming at lowering the growth temperature, is of importance and motivates much recent work, including the studies presented in this thesis.

2. Growth of alumina – role of energetic bombardment

In order to lower the growth temperatures of crystalline alumina coatings, researchers have turned to PVD techniques. Notably, Zywitzki *et al.*[69] used pulsed DC sputtering and grew single-phase α-alumina films at 760 °C, significantly lower than both the CVD temperatures and the θ-α transformation temperature. By ionized PVD Schneider *et al.*[70, 71] grew κ-alumina at temperatures as low as 430 °C, by applying a negative bias on the substrate to increase the energy of the depositing species and to bombard the growing film with sputtering gas ions. Kyrylov *et al.*[72] used plasma assisted CVD to grow α-alumina at 580 °C, and in Paper I and II α-alumina films were grown by magnetron sputtering at temperatures down to 280 °C with the use of chromia nucleation layers. An important reason for these rather dramatic decreases in growth temperatures is *energetic bombardment*, which can be more or less controllably used in deposition situations involving a plasma.

As stated in Section II.A.7, bombardment during growth can strongly influence the structure and properties of thin films. Recently a few studies have appeared, studying the role of energetic bombardment during cathodic vacuum arc deposition of alumina thin films.[29,73,74] These works show that it is possible to promote crystalline phase formation and that the deposition temperature of α-alumina can be decreased from 800-900 °C to 600-700 °C by applying a high substrate bias (< -100 V). In this kind of deposition technique the ion-to-neutral ratio is large so that a high bias implies a high kinetic energy of the depositing species. In the conventional magnetron sputtering, as used in this work, the degree of ionization is low. However, we still believe that the apparent promotion of α-alumina formation (Papers I and II) was due to bombardment by energetic oxygen ions/atoms in combination with nucleation control. The oxygen are formed during sputtering of oxides at the target surface as negative ions and are accelerated away from the target towards the substrate.[17,19,20] If they do not suffer collisions in the plasma, they will bombard the growth surface with energies of a few hundred eV (corresponding to the target sheath voltage).

3. Growth of alumina – role of surfaces

Another fundamental area of alumina growth has also been elucidated recently. At initial growth, surface energies are of great importance, since the relative surface area of small grains is large. McHale *et al.*[2] measured the surface energy of γ- and α-alumina and concluded that for surface areas of above 125 m^2/g, the γ phase is energetically favored due to its much lower surface energy (for a spherical γ-alumina grain this value corresponds to a grain diameter of about 13 nm). These measurements, which confirmed the predictions made by Blonski and Garofalini[75] by atomistic computer simulations, lead to the suggestion that the metastable aluminas are *surface energy stabilized* at initial growth, i.e., they form because they are thermodynamically stable when the grain size is small enough. In order for a transformation to the α phase to occur, the growth temperature must be raised to initiate bulk diffusion or the growth surface must be bombarded as discussed in the previous section. Ruppi[65] has recently shown that by controlling the nucleation step high quality α- or κ-alumina can be grown by CVD at 1000 °C. This demonstrates that the nucleation step is highly important also at high growth temperatures.

In Papers I and II the substrate is chosen to promote α nucleation, and we show that it is then possible to grow the α phase at low temperatures (280 °C) by magnetron sputtering. Thus, as seen from this and the previous section, successful deposition of α-alumina thin films at low temperatures can be achieved by controlling both the nucleation step of growth and the energy supplied to the growth surface through bombardment.

4. Theoretical studies of alumina

A fundamental understanding of many growth-related phenomena can be reached only by studying the material on an atomic scale. This is the driving force for performing atomistic computer calculations. However, due to the time cost of accurate calculations they are limited to very small (and idealized) systems. The present evolution, to decrease the gap in scales between experiments and computer calculations, will surely revolutionize the use of computational methods in materials industry and research.

Concerning alumina, it seems that for many close to ideal situations (e.g., perfect bulk or clean surfaces), a classical picture, such as classical molecular dynamics (MD), gives a good description of its properties. A reason for this is the high degree of ionicity of the oxide, implying that the atoms can be thought of as spherical ions interacting via almost purely electrostatic forces. This simple picture seems to be fairly accurate for alumina and can be

accurately described by a computationally effective classical potential. An example is the previously mentioned calculations on α and γ surfaces by Blonski and Garofalini,[75] which were later confirmed experimentally.[2] Other examples are simulations of liquid[76,77] and amorphous[78] alumina using a simple pair potential originally intended for crystalline materials,[79] but producing results fitting very nicely with experiment even in these non-perfect situations. However, such potentials are limited to the ionic situations, since they assume a constant charge of the ions. In order to accurately describe, e.g., metal oxidation or surface diffusion on alumina, a model that allows for charge transfer must be used.[80]

Following the increasing performance of computers, the use of *ab initio* (i.e., from first principles) quantum mechanical models, such as DFT, have increased immensely during the last decade. These methods open the possibilities for studies on, e.g., various compositions and configurations, ideal or not, with high accuracy and without the need for potentials that are fitted to previously known material properties. In studies on alumina, this has resulted in numerous works using DFT on bulk,[81,82,83] surfaces,[84,85,86] ad-atoms,[84,85,87] Al oxidation,[88] interfaces,[89] phase transformations,[90] phase stability,[81,82] phase determination,[91] doping,[92,93] etc. Recently, also *ab initio* molecular dynamics calculations were performed studying ion-surface interactions during low-energy bombardment of the α-alumina surface.[94]

A common feature of the many static bulk DFT calculations on alumina is their consistency of results and very good agreement with experiments on, e.g., structural parameters. The only general discrepancies are an underestimation of lattice parameters with LDA calculations and an overestimation with the GGA, but the errors are only of the order of 1% and common for DFT calculations. Corresponding deviations are seen in calculated bulk moduli values, suggesting that the LDA and GGA tend to predict too strong and too weak chemical bonding, respectively.

DFT calculations on energy differences between phases are typically fairly accurate, but in the alumina case they are complicated by the fact that the differences are very small. For example, Lodziana and Parlinski[82] calculated a difference between α and θ of only 0.03 eV/fu (fu = chemical formula unit) with the GGA. Wolverton and Hass[81] report a similar value of 0.04 eV/fu by GGA calculations and 0.25 eV/fu within the LDA. These can be compared to an experimental value of 0.12 eV/fu for the energy difference between α and δ, as reported by Yokokawa and Kleppa.[95] Since δ is claimed to transform to α via the θ phase, this value should set an upper limit on the α-θ energy difference. Thus, it seems that only the

GGA results are consistent with experiment. However, when comparing, e.g., the effects of doping on the energy difference, GGA and LDA give similar results, as seen in Paper V.

5. The effect of doping on alumina phase stability

Due to the application of the metastable aluminas as catalysts or catalyst supports, there is an interest in stabilizing them with respect to the α phase. A natural course of action, taken by a number of researchers, would be to investigate the effects of dopants on the relative phase stability.

Most dopants attempted in previous works seem to retard the γ-α transformation (e.g., Cr,[96,97,98] Cs,[99] B,[100] La,[101,102] Ce,[101,102] Ba,[103] Sr,[103] Ca,[103] Er,[97] Y[97]), but not stop it. These authors suggest that the reason for these effects is that the ions block diffusion and thus delays and/or slows the transformation towards the stable α phase. However, they do not report where the dopants are situated within the material and thus questions arise: is diffusion blocking actually the governing mechanism for transformation retardation? If it is, where does it take place? What effect on alumina phase stability do the dopants have if they are substituted into the lattice?

The latter question is addressed in Papers V and VI, which deals with the effect of substitutional dopants on the stability of α- and θ-alumina, as calculated within DFT. There are no such calculations available in the literature, but there are a few that deal with doping of alumina from other points of view. Haverty *et al*.[92] studied transition metal doping of κ-alumina. Their results show a preference for octahedral positions for the tested dopants (Nb, Zr, Y, Sc), due to their larger ionic radius compared to Al.[104] Verdozzi *et al*.[93] showed that a La impurity in the α-alumina lattice is displaced by 0.5 Å from the corresponding Al position. This demonstrates the difficulty to incorporate a large ion into the dense α phase, but none of these studies report results on the stability of doped alumina. The next chapter summarizes the work done in the appended papers, including the results from our work on doped alumina.

V. CONTRIBUTION TO THE FIELD

The work done and presented in the appended papers is motivated by the problems of alumina growth and phase stability, as discussed in the previous chapters. Hopefully, the studies performed during this thesis work give some answers, expand some questions, and contribute towards a fundamental understanding of alumina thin film growth. In the following a brief overview of the work presented in the appended papers is given.

A. Thin film growth and characterization (Papers I and II)

As described in Chapter IV, growth of α-alumina typically requires temperatures above 1000 °C. With refined deposition techniques, the growth temperatures were further lowered to 760 °C by pulsed DC sputtering,[69] 580 °C by plasma assisted CVD,[72] and for the κ phase even to 430 °C by ionized PVD.[24] These results were the result of supplying energy to the growth surface by means of ion bombardment, compensating for the energy lost by lowering the temperature.

In this work α-alumina films were grown onto pre-deposited chromia layers using RF magnetron sputtering.[105] In Paper I ceramic alumina targets were used, while in Paper II the films were grown by reactive sputtering of Al in an $Ar+O_2$ gas mixture. The results show that dense, hard, and single phased α-alumina thin films can be grown at temperatures down to 280 °C. The reasons for the dramatic decrease in growth temperature are twofold. Firstly, the

pre-deposited chromia layers act as “templates” for α phase growth, due to the isomorphism of chromia and α-alumina with a relatively small lattice mismatch. This further supports the importance of the surface energy in the initial steps of growth (see also Section IV.B.3). In other words, when using an amorphous substrate the metastable phases form, since they are surface energy stabilized,[2] but if α phase nucleation is promoted, e.g., through a template layer, α-alumina can be grown even at low temperatures. Secondly, α phase formation was shown (Paper II) to be induced by energetic bombardment of the growth surface by depositing species. Similar effects have been observed before at higher temperatures by applying high bias voltages in ionized PVD cathodic arc evaporation experiments (see Section IV.B.2). In the present case, we conclude (supported also by the results of Paper IV) that energetic oxygen is the most likely cause of α phase promotion. This conclusion is due to the dependence on film crystal structure on the total and O_2 partial pressures. At relatively high total pressure (0.67 Pa) only γ-alumina formed, since the energetic bombardment decreased, while at 0.33 Pa the α phase could be grown. Furthermore, α-alumina formation occurred only as the O_2 pressure was high enough (in the later stage of the transition to the oxidized target mode). This is the same O_2 pressure region in which the production of energetic oxygen increases dramatically, which leads to the conclusion that they are responsible for the change in crystalline phase.

In conclusion, *low-temperature deposition of α-alumina is shown to be possible by controlling both the nucleation step of growth as well as the energetic bombardment of the growing film.*

B. Plasma analysis (Papers III and IV)

A thin film is formed through chemical bonding between the species incident onto the substrate. Thus, knowledge of the contents of the deposition flux is of immense importance in order to understand and control the growth. Moreover, as seen above, knowledge of the energies of the depositing species is of high interest. In Papers III and IV the contents and energy distributions, respectively, of the depositing species are studied by energy-resolved mass spectrometry.

During sputter deposition of oxides it is likely that the deposition flux contains not only atomic species, but also molecules. The measurements presented in Paper III showed indeed that the ionic deposition flux during reactive magnetron sputtering contained up to about 10% AlO^+, relative to Al^+, as the O_2 partial pressure was increased. Due to the much

higher ionization probability of Al, the amounts of neutral AlO were estimated to be similar to, or even higher than, the amounts of Al. These results are of fundamental importance in the further understanding of alumina growth, even though no clear correlations to film growth were found in this work.

Paper IV contains investigations of ion energy distributions of the ions incident onto the substrate. The positive ions of the film-forming species exhibited bimodal distributions, where the low-energy peak is interpreted as corresponding to thermalized ions, accelerated from the plasma potential. The second (high-energy) peak seems to originate from sputtered particles retaining their energy from the sputtering event. During DC sputtering this peak appears at an energy of about 5 eV relative to the plasma potential peak, while in RF sputtering the peak energy is higher and the distributions appear more complex, most likely due to RF modulations of the ion energies. The energy distributions of the negative oxygen ions were also measured, showing a distinct peak at low pressure (0.33 Pa), corresponding to ions which have been accelerated over the target sheath potential and reached the mass spectrometer (situated at a typical substrate position) without collisions. This peak increases strongly as the O_2 partial pressure increases, and diminishes at higher total pressure, supporting the conclusion of Paper II that energetic oxygen is responsible for promoting α-alumina formation.

C. DFT calculations on alumina phase stability (Papers V and VI)

In Chapter IV, some of the previous research done on doping of alumina was reviewed. Many researchers have explored the idea of doping, often with the aim to thermally stabilize the metastable aluminas. These studies typically draw conclusions concerning the effect of the dopants on the kinetics and speed of the transformation to the α phase. There are also some theoretical studies on doping, aiming at, e.g., improved electrical properties. However, none of these studies have investigated the effects of the dopants on energetics, or phase stability, between alumina phases.

In Papers V and VI, the effects of doping on θ- and α-alumina stability are calculated within DFT. This is done through substitutionally replacing one Al (or O) atom in the alumina lattices with a dopant atom, resulting in a doping level of 5 at.% (20-atom supercell). Among the tested dopant ions it is clear that those that are significantly larger than aluminum, such as Mo, tend to stabilize the less dense θ phase and even make it energetically stable relative to the α phase. This implies that the transformation to the α phase should not take

place at all at the studied amount of substitutional doping. However, this is true only if the dopants remain within the θ lattice; we also show (Paper VI) that it is energetically favorable for doped alumina to be separated into pure alumina and other phases, containing the dopants. Thus, *doping can have a strong stabilizing effect on the metastable aluminas, but phase separation will most likely occur at high temperatures.* The overall result in an experimental situation might be a retardation of the transformation to the α phase.

From the point of view of our experimental work, it would also be of interest to destabilize the metastable aluminas, i.e., to investigate if α phase formation can be promoted by doping. Among the tested dopants, Co and Cu were found to increase the energy difference between the phases. The shifts are rather small in absolute numbers, but could still be important since the energy difference for pure alumina is also small. Growth studies and/or calculations investigating the effect on surface energies would have to be performed in order to draw further conclusions on the possibilities of promoting α phase formation by doping.

REFERENCES

[1] W.H. Gitzen, *Alumina as a ceramic material* (The American Ceramic Society, Westerville, 1970), p. 3.

[2] J.M. McHale, A. Auroux, A.J. Perotta, and A. Navrotsky, Science 277, 788 (1997).

[3] M. Ohring, *The Materials Science of Thin Films* (Academic Press, San Diego, 1992), pp. 101-118.

[4] P. Sigmund, Phys. Rev. 184, 383 (1969).

[5] S. Maniv and W.D. Westwood, J. Vac. Sci. Technol. 17, 743 (1980).

[6] B. Chapman, *Glow Discharge Processes* (Wiley, New York, 1980), pp. 49-76.

[7] M. Ohring, *The Materials Science of Thin Films* (Academic Press, San Diego, 1992), pp. 123-126.

[8] M. Ohring, *The Materials Science of Thin Films* (Academic Press, San Diego, 1992), pp. 121-123.

[9] See, e.g., S. Berg and T. Nyberg, Thin Solid Films 476, 215 (2005).

[10] See, e.g., W.D. Sproul, D.J. Christie, and D.C. Carter, Thin Solid Films 491, 1 (2005).

[11] M.W. Thompson, Phil. Mag. 18, 377 (1968).

[12] W.O. Hofer in *Sputtering by Particle Bombardment III* (ed. R. Behrisch and K. Wittmaack, Springer-Verlag, Berlin, 1991), pp.54-67.

[13] R.V. Stuart and G.K. Wehner, J. Appl. Phys. 35, 1819 (1964).

[14] R.V. Stuart, G.K. Wehner, and G.S. Anderson, J. Appl. Phys. 40, 803 (1969).

[15] A. Cortona, W. Husinsky, and G. Betz, Phys. Rev. B 59, 15495 (1999).

[16] M.L. Yu, D. Grischkowsky, and A.C. Balant, Phys. Rev. Lett. 48, 427 (1982).

[17] D.J. Kester and R. Messier, J. Vac. Sci. Technol. A 4, 496 (1986).

[18] K. Tominaga, S. Iwamura, Y. Shintani, and O. Tada, Jpn. J. Appl. Phys. 21, 688 (1982).

[19] K. Tominaga, T. Murayama, Y. Sato, and I. Mori, Thin Solid Films 343-344, 81 (1991).

[20] T.I. Selinder, G. Larsson, U. Helmersson, and S. Rudner, J. Appl. Phys. 69, 390 (1991).

[21] J. Neidhart, B. Abendroth, R. Gago, W. Möller, and L. Hultman, J. Appl. Phys. 94, 7059 (2003).

[22] J.W. Coburn, E. Taglauer, and E. Kay, Jpn. J. Appl. Phys. Suppl. 2, Pt. 1, 501 (1974).

[23] J.A. Thornton, J. Vac. Sci. Technol. 11, 666 (1974); J. Vac. Sci. Technol. A 4, 3059 (1986).

[24] J.M. Schneider, W.D. Sproul, A.A. Voevodin, and A. Matthews, J. Vac. Sci. Technol. A 15, 1084 (1997).

[25] I. Petrov, L. Hultman, U. Helmersson, J.-E. Sundgren, and J.E. Greene, Thin Solid Films 169, 299 (1989).

[26] L. Hultman, W.-D. Münz, J. Musil, S. Kadlec, I. Petrov, and J.E. Greene, J. Vac. Sci. Technol. A 9, 434 (1991).

[27] L. Hultman, S.A. Barnett, J.-E. Sundgren, and J.E. Greene, J. Cryst. Growth 92, 639 (1988).

[28] J.E. Greene and S.A. Barnett, J. Vac. Sci. Technol. 21, 285 (1982).

[29] J. Rosén, S. Mráz, U. Kreissig, D. Music, and J.M. Schneider, Plasma Chem. Plasma Processing 25, 303 (2005).

[30] S.M. Rossnagel and J. Hopwood, J. Vac. Sci. Technol. B 12, 449 (1994).

[31] V. Kouznetsov, K. Macak, J.M. Schneider, U. Helmersson, and I. Petrov, Surf. Coat. Technol. 122, 290 (1999).

[32] P.O.Å. Persson, Ph.D. Thesis (Linköping Studies in Science and Technology, dissertation no. 695, Linköping University, Sweden, 2001).

[33] W.C. Oliver and G.M. Pharr, J. Mater. Res. 7, 1564 (1992).

[34] See, e.g., J.E.E. Baglin and J.S. Williams in *Ion Beams for Materials Analysis* (ed. J.R. Bird and J.S. Williams, Academic Press, Marrickville, 1989), pp. 144-148.

[35] P. Hohenberg and W. Kohn, Phys. Rev. 136, B864 (1964).

[36] W. Kohn and L.J. Sham, Phys. Rev. 140, A1133 (1965).

[37] R.M. Martin, *Electronic Structure – Basic Theory and Practical Methods* (Cambridge University Press, Cambridge, 2004).

[38] M. Sprik in *Classical and Quantum Dynamics in Condensed Phase Simulations* (World Scientific, Singapore, 1998), pp. 285-309.

[39] C. Ruberto, Ph.D. Thesis (Chalmers University of Technology, Göteborg, Sweden, 2001).

[40] J.P. Perdew and Y. Wang, Phys. Rev. B 45, 13244 (1992).

[41] J.P. Perdew, J.A. Chevary, S.H. Vosko, K.A. Jackson, M.R. Pederson, D.J. Singh, and C. Fiolhais, Phys. Rev. B 46, 6671 (1992).

[42] G. Kresse and D. Joubert, Phys. Rev. B 59, 1758 (1999).

[43] D. Vanderbilt, Phys. Rev. B 41, 7892 (1990).

[44] P.E. Blöchl, Phys. Rev. B 50, 17953 (1994).

[45] G. Kresse and J. Furthmüller, Phys. Rev. B 54, 11169 (1996).

[46] More information about the package is available through the VASP group web page, http://cms.mpi.univie.ac.at/vasp/.

[47] I. Levin and D. Brandon, J. Am. Ceram. Soc. 81, 1995 (1998).

[48] W.H. Gitzen, *Alumina as a ceramic material* (The American Ceramic Society, Westerville, 1970), pp. 31, 46, 64.

[49] Y. Sato and S. Akimoto, J. Appl. Phys. 50, 5285 (1979).

[50] R.W.G. Wyckoff, *Crystal Structures*, 2nd ed., vol. 2 (Interscience, New York, 1964), pp. 13-14.

[51] W.H. Gitzen, *Alumina as a ceramic material* (The American Ceramic Society, Westerville, 1970), p. 17.

[52] Y.-N. Xu and W.Y. Ching, Phys. Rev. B 43, 4461 (1991).

[53] R.W.G. Wyckoff, *Crystal Structures*, 2nd ed., vol. 2 (Interscience, New York, 1964), pp. 6-8.

[54] C. Kittel, *Introduction to Solid State Physics* (Wiley, New York, 1996), pp. 91-92.

[55] L. Karlsson, L. Hultman, and J.-E. Sundgren, Thin Solid Films 371, 167 (2000).

[56] J. Müller, M. Schierling, E. Zimmermann, and D. Neuschütz, Surf. Coat. Technol. 120-121, 16 (1999).

[57] R.H. French, J. Am. Ceram. Soc. 73, 477 (1990).

[58] R.-S- Zhou and R.L. Snyder, Acta. Cryst. B 47, 617 (1991).

[59] A.P. Borosy, B. Silvi, M. Allavena, and P. Nortier, J. Phys. Chem. 98, 13189 (1994).

[60] R. Franchy, G. Schmitz, P. Gassmann, and F. Bartolucci, Appl. Phys. A 65, 551 (1997).

[61] Z.R. Ismagilov, R.A. Shkrabina, and N.A. Koryabkina, Catal. Today 47, 51 (1999).

[62] S.-D. Mo, Y.-N. Xu, and W.-Y. Ching, J. Am. Ceram. Soc. 80, 1193 (1997).

[63] J.-E. Sundgren, Ph.D. Thesis (Linköping Studies in Science and Technology, dissertation no. 79, Linköping University, Sweden, 1982).

[64] O. Knotek, M. Böhmer, and T. Leyendecker, J. Vac. Sci. Technol. A 4, 2695 (1986).

[65] S. Ruppi, Int. J. Refract. Met. Hard Mater. 23, 306 (2005).

[66] H.G. Prengel, W. Heinrich, G. Roder, and K.H. Wendt, Surf. Coat. Technol. 68-69, 217 (1994).

[67] M. Halvarsson and S. Vuorinen, Surf. Coat. Technol. 76-77, 287 (1995).

[68] J. Müller, M. Schierling, E. Zimmermann, and D. Neuschütz, Surf. Coat. Technol. 120-121, 16 (1999).

[69] O. Zywitzki, G. Hoetzsch, F. Fietzke, and K. Goedicke, Surf. Coat. Technol. 82, 169 (1996).

[70] J.M. Schneider, W.D. Sproul, A.A. Voevodin, and A. Matthews, J. Vac. Sci. Technol. A 15, 1084 (1997).

[71] J.M. Schneider, Ph.D. Thesis, (University of Hull, 1997).

[72] O. Kyrylov, D. Kurapov, and J.M. Schneider, Appl. Phys. A 80, 1657 (2004).

[73] Q. Li, Y.-H. Yu, C. Singh Bhatia, L.D. Marks, S.C. Lee, and Y.W. Chung, J. Vac. Sci. Technol. A 18, 2333 (2000).

[74] R. Brill, F. Koch, J. Mazurelle, D. Levchuk, M. Balden, Y. Yamada-Takamura, H. Maier, and H. Bolt, Surf. Coat. Technol. 174-175, 606 (2003).

[75] S. Blonski and S.H. Garofalini, Surf. Sci. 295, 263 (1993).

[76] R. Ahuja, A.B. Belonoshko, and B. Johansson, Phys. Rev. E 57, 1673 (1998).

[77] G. Gutierrez, A.B. Belonoshko, R. Ahuja, and B. Johansson, Phys. Rev. E 61, 2723 (2000).

[78] G. Gutierrez and B. Johansson, Phys. Rev. B 65, 104202 (2002).

[79] M. Matsui, Phys. Chem. Minerals 23, 345 (1996).

[80] F.H. Streitz and J.W. Mintmire, Phys. Rev. B 50, 11996 (1994).

[81] C. Wolverton and K.C. Hass, Phys. Rev. B 63, 24102 (2000).

[82] Z. Lodziana and K. Parlinski, Phys. Rev. B 67, 174106 (2003).

[83] Y. Yourdshahyan, C. Ruberto, L. Bengtsson, and B.I. Lundqvist, Phys. Rev. B 56, 8533 (1997).

[84] C. Verdozzi, D.R. Jennison, P.A. Schultz, and M.P. Sears, Phys. Rev. Lett. 82, 799 (1999).

[85] X.-G. Wang, A. Chaka, and M. Scheffler, Phys. Rev. Lett. 84, 3650 (2000).

[86] C. Ruberto, Y. Yourdshahyan, and B.I. Lundqvist, Phys. Rev. B 67, 195412 (2003).

[87] A. Bogicevic and D.R. Jennison, Phys. Rev. Lett. 82, 4050 (1999).

[88] D.R. Jennison, C. Verdozzi, P.A. Schultz, and M.P. Sears, Phys. Rev. B 59, R15605 (1999).

[89] A. Christensen and E.A. Carter, Phys. Rev. B 62, 16968 (2000).

[90] S.-H. Cai, S.N. Rashkeev, S.T. Pantelides, and K. Sohlberg, Phys. Rev. Lett. 89, 235501 (2002).

[91] Y. Yourdshahyan, C. Ruberto, M. Halvarsson, L. Bengtsson, V. Langer, and B.I. Lundqvist, J. Am. Ceram. Soc. 82, 1365 (1999).

[92] M. Haverty, A. Kawamoto, K. Cho, and R. Dutton, Appl. Phys. Lett. 80, 2669 (2002).

[93] C. Verdozzi, D.R. Jennison, P.A. Schultz, M.P. Sears, J.C. Barbour, and B.G. Potter, Phys. Rev. Lett. 80, 5615 (1998).

[94] J. Rosén, J.M. Schneider, and K. Larsson, Solid State Commun. 135, 90 (2005).

[95] T. Yokokawa and O.J. Kleppa, J. Phys. Chem. 68, 3246 (1964).

[96] D.R. Clarke, Phys. Stat. Sol. A 166, 183 (1998).

[97] D.D. Ragan, J. Am. Ceram. Soc. 86, 541 (2003).

[98] G.C. Bye and G.T. Simpkin, J. Am. Ceram. Soc. 57, 367 (1974).

[99] K. Okada, A. Hattori, Y. Kameshima, and A. Yasumori, Mater. Lett. 42, 175 (2000).

[100] T.-D. Chen, L. Wang, H.-R. Chen, and J.-L. Shi, Mater. Lett. 50, 353 (2001).

[101] Z.R. Ismagilov, R.A. Shkrabina, and N.A. Koryabkina, Catal. Today 47, 51 (1999).

[102] M. Ozawa, M. Kimura, and A. Isogai, J. Mater. Sci. Lett. 9, 709 (1990).

[103] A. Douy, Key Eng. Mater. 132-136, 101 (1997).

[104] R.D. Shannon, Acta Cryst. A 32, 751 (1976).

[105] P. Jin, G. Xu, M. Tazawa, K. Yoshimura, D. Music, J. Alami, and U. Helmersson, J. Vac. Sci. Technol. A 20, 2134 (2002).